VELOCITY MEASUREMENTS IN NASAL CAVITIES BY MEANS OF STEREOSCOPIC PIV - PRELIMINARY TESTS

2017 J. Phys.: Conf. Ser. 882 012010

(http://iopscience.iop.org/1742-6596/882/1/012010)

IOP Conf. Series: Journal of Physics: Conf. Series **882** (2017) 012010 doi:10.1088/1742-6596/882/1/012010

VELOCITY MEASUREMENTS IN NASAL CAVITIES BY MEANS OF STEREOSCOPIC PIV - PRELIMINARY TESTS

Fabio Cozzi[1,4], Giovanni Felisati[2], Maurizio Quadrio[3]

[1] Department of Energy, Politenico di Milano, Via Lambruschini 4, 20156, Milan, Italy
[2] Otorhinolaryngology Unit, Head and Neck Department, San Paolo Hospital, Università degli Studi di Milano, Via di Rudinì 8, 20142 Milan, Italy
[3] Department of Aerospace Sciences and Technologies, Politecnico di Milano, Via La Masa 34, 20156 Milan, Italy

[4]Corresponding author: fabio.cozzi@polimi.it

Abstract. The prediction of detailed flow patterns in human nasal cavities using computational fluid dynamics (CFD) can provide essential information on the potential relationship between patient-specific geometrical characteristics of the nasal anatomy and health problems, and ultimately led to improved surgery. The complex flow structure and the intricate geometry of the nasal cavities make achieving such goals a challenge for CFD specialists. The need for experimental data to validate and improve the numerical simulations is particularly crucial. To this aim an experimental set-up based on Stereo PIV and a silicon phantom of nasal cavities have been designed and realized at Politecnico di Milano. This work describes the main features and challenges of the set-up along with some preliminary results.

1. Introduction

The human nasal cavity is devoted to several important physiological functions such as: filtering, warming and humidifying of the inspired air before it reaches the lungs and to facilitate the sense of smell. The nasal cavity is also important for taste. Any dysfunction of this organ causes a reduction in the personal comfort, and often surgery is employed to eliminate or just to alleviate such problems. Nasal breathing difficulties (NBD) represent one of the most common medical conditions, afflicting tens of million people and accounting for billions of Euros in health-care costs annually [1,2]. The surgery approach is hindered to a various extent by the incomplete knowledge of the behavior of the air-flow along the nasal cavity; any improvement in this respect would lead to better surgery planning and greater effectiveness: i.e. benefits for the patient and significant costs reductions for the healthcare system. From this point of view, computational fluid dynamics (CFD) in principle enables detailed prediction of flow patterns in nasal cavities and provides essential information on the potential relationship between patient-specific geometrical characteristics and health problems. Obviously, the daily clinical practice requires the numerical model to be not only accurate but also able to provide useful results in a reasonably short time. The complex flow structure along with the intricate geometry of the nasal anatomy pose significant challenges if one sets out to achieve such goals.

Experimental data to validate and improve the numerical simulations are particularly needed in this context, and at the same time particularly difficult to obtain, as *in-vivo* measurements are nearly impossible. Hence, an experimental set-up based on Stereo PIV (SPIV) and a silicon phantom of nasal cavities has been designed and realized at Politecnico di Milano. To the authors' knowledge, the very few literature works concerned with *in-vitro* experiments analyzing the airflow inside the upper airways have so far considered only the main passageways, excluding the large volumes of the paranasal sinuses, see for example [3,4,5]. Instead we decided to build an anatomically consistent model which retains the entire air volumes, i.e. the full anatomy of the human nose, including the whole region of the paranasal sinuses, which are obviously very important in treating NBD in general, and in planning a FESS (Functional Endoscopic Sinus Surgery) in particular. The present paper describes the approach followed to develop an experimental set-up, based on S-PIV and refractive index matching technique, to analyze the airflow inside a complete silicon model of the human nose. Preliminary results and a comparison with a Large Eddy Simulation on the same anatomy are presented and briefly analyzed.

2. Experimental set-up and Techniques

2.1. The Refractive Index Matching technique

A perfectly transparent model is needed if Particle Image Velocimetry (PIV) technique has to be used. Nevertheless nasal cavities have a quite complex geometry with irregular shapes and curved wall, so even in a perfectly transparent model the mismatch between the refractive index of themodel and that of the fluid (air) generates strong optical distortion preventing the use of quantitative image-based techniques. Budwing presented a robust method for eliminating refraction of light passing through model and/or test section walls [6]. The method consists in replacing the actual fluid with one that matches the refractive index of the solid transparent object (i.e. the model or the walls) and it is known as refractive index matching (RIM) technique. Organic liquids, liquid mixtures or aqueous solutions can be used as matching fluid [6,7,8]. The RIM makes the refractive index field spatially homogeneous eliminating any optical distortion. In our case the transparent model is totally submerged in a large box containing the matching fluid. By this way the model becomes optically invisible inside the box and one can shoot the laser through the model, or look through it, without optical artifacts. Being the model disappeared in the fluid, it is called "Phantom model". To simulate the breathing cycle a volumetric pump is connected to the model in such a way to allow the fluid to be inhaled/exhaled through the nostrils of the model.

2.2. The Phantom Head.

The actual size of the model was determined after an accurate analysis of the many factors involved in such a decision. The final size (in a 2:1 scale, i.e. the model is exactly twice the real dimensions) is a weighted compromise among several factors: a larger model reduces flow velocities, increases the gaps, and improves PIV resolution, but comes at various costs, including increased size, weight and money.

The geometry of the nasal cavity is reconstructed from the head CT scan of a 67-year-old male patient who showed a normal sinonasal anatomy. The patient underwent a plain head CT scan with a 64-row multi-detector CT. The scanner has a 512 × 512 matrix, accounting for a 0.49 mm × 0.49 mm spatial resolution in the sagittal–coronal plane and a 0.625 mm gap between consecutive axial slices. The images from the CT scan are first manipulated with the open-source software 3D-Slicer [9]. 3D-Slicer is used to convert the CT images into an accurate geometrical description of the boundary of the volume of interest, through image segmentation and volume reconstruction. After selecting the volume of interest and segmenting the image, the reconstructed three-dimensional geometry is exported and saved into a STereoLithography (STL) file. A limited amount of smoothing is applied to the reconstructed surface before exporting to STL, to avoid small-scale irregularities. The chosen anatomy, and the employed STL file, can then be used in the numerical simulations. This is a key step

for enabling in the future a quantitative one-to-one comparison between numerical and experimental results.

At first the shape of the air volume (in analogy with the lost-wax casting technique) is produced and then the model is eventually casted into transparent silicone. The used 3D-printing technology allowed a spatial accuracy much better than the slice thickness of the CT scan while using as a printing material a water-dissolvable substance. Among the other technical characteristics, the printer has a resolution of 600x540 dpi, and prints details down to 100 micron size, with a building speed of 28mm/hour and a 254x381x203 working volume, that is just enough for our model. The printing material is demihydrathed calcium solphate, that is easily dissolved in water. Once printed, the model is carefully coated with a blue-colored, diluted vinil-based glue in preparation to the silicone casting. For the silicone we have adopted the very stable Sylgard 184 silicone elastomer, according to the manufacturer it has a refractive index of n = 1.4118 @ 589 nm [10]. A Plexiglas-made container box has been realized for the casting process. When ready for casting, the two components of the silicone are well mixed and degassed before pouring into the box. The curing process lasts a few days at room temperature. The blue-coated model within the casting box filled by silicone is shown in figures 1(a)-(b). Figure 2(a) shows the model once extracted from the casting box, before the start of the long and delicate process of removal of the internal material, and figure 2(b) shows the fully cleaned model.

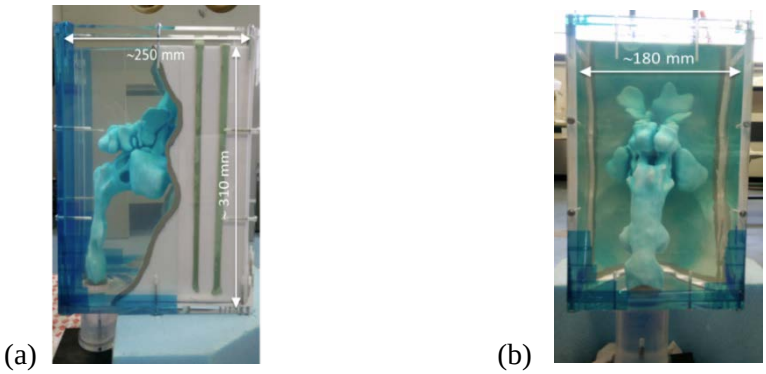

Figure 1. The silicone model inside the casting box. The nasal anatomy is evidenced by the blue coated printed material. (a) Side view, (b) front view.

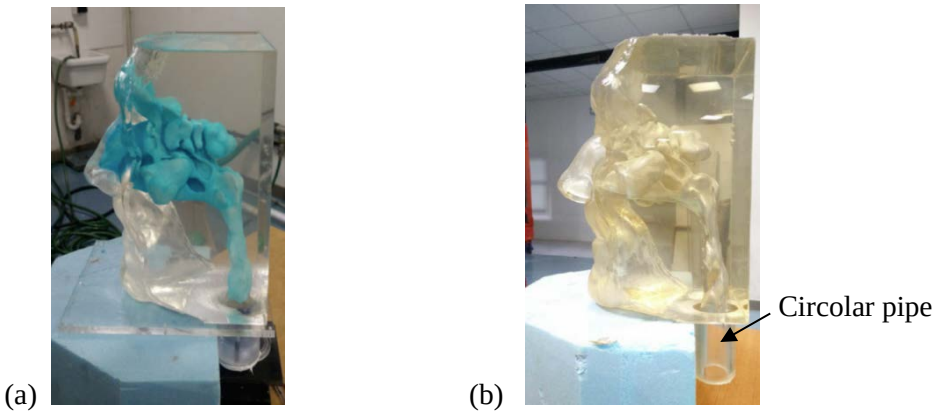

Figure 2. The silicone model once removed from the casting box. (a) Before removal of the internal material, (b) the cleaned model.

The printing material was hard to remove using only water, and a 5% Acetic Acid in water solution worked much better. Unfortunately the model suffered of few small damages due to a first attempt to mechanically remove the printing material and lastly, once cleaned, the model yellowed, figure 2(b). Anyhow these issues didn't compromise the optical clarity of the model allowing the experimental activity to be carried out. As shown in figure 2(b), the laryngopharynx of the cast model is extended in

a circular pipe of about 50 mm in diameter and 100 mm in length to allow the pumping system to be connected to the model.

2.3. Fluid choice and properties

2.3.1. Refractive Index. As a first requirements the working fluid has to match the refractive index of the model. Following the work of Spence et al. [3] we chose as a matching fluid a mixture of water and glycerol. The latter is a non-toxic, clear liquid with a high refractive index and viscosity [11]. Being commonly used in the food industry glycerin is inexpensive and it is also compatible with materials commonly used in the phantom, flow circuit and pump [11]. The refractive index of the mixture, n_{mix}, can be quite easily controlled by adjusting water fraction and temperature. For their phantom model Spence et al. used a matching mixture composed by 39% water and 61% glycerin by volume [3], the same matching mixture is reported by Geoghegan et al. for phantom made of Sylgard 184 [11].

The refractive index of a binary mixture, n_{mix}, can be estimated through the use of mixture rules [7]. For water-glycerin mixture the simplest one is based on the Gladstone-Dale relationship and it gives n_{mix} as per equation (1):

$$n_{mix} - 1 = \left(n_{H_2O} - 1\right) X_{H_2O} + \left(n_{Glyc} - 1\right) X_{Glyc} \tag{1}$$

where n_{H_2O} is the refractive index of water, n_{Glyc} is the refractive index of glycerin, X_{H_2O} is the volume fraction of water, and X_{Glyc} is the volume fraction of glycerin. Another commonly used mixture rule is based on the Lorentz-Lorentz equation and shown in equation (2).

$$\left(\frac{n_{mix}^2 - 1}{n_{mix}^2 + 2}\right) = \left(\frac{n_{H_2O}^2 - 1}{n_{H_2O}^2 + 2}\right) X_{H_2O} + \left(\frac{n_{Glyc}^2 - 1}{n_{Glyc}^2 + 2}\right) X_{Glyc} \tag{2}$$

To check their accuracy, the refractive index of the water-glyceryn estimated using both equations (1) and (2) was compared to the value measured at 298.15 K and 589.3 nm by Vural et al [12]. The values $n_{H_2O} = 1.3334$ and $n_{Glyc} = 1.4729$ taken from [12] are used in both equations, while volume fractions are estimated from mass fractions and pure fluids density.

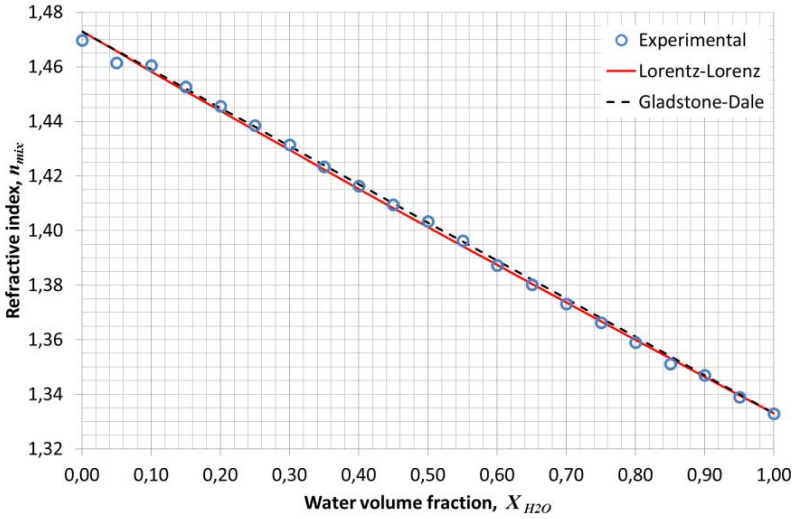

Figure 3. Comparison between the experimental values of n_{mix} (empty symbol) [12] and those predicted by equation (1) (dashed line) and equation (2) (solid line).

Results shown in figure 3 evidenced that both mixture rules work fine in predicting the measured n_{mix}. Equation (1) can be preferable being more simple, anyhow equation (2) shows a slightly better agreement with the experimental data. According to equation (2) the fluid used by Spencer et al. and by Geoghegan et al. has n_{mix} =1.417. On the other side the manufacturer quotes a refractive index of n_{syl} = 1.4118 @ 589 nm for the Sylgard 184 [10], while Geoghegan et al. reports n_{syl} = 1.43 for the same material without specifying at which wavelength [11]. The refractive index of the cured material depends on the mixing and curing processes, so the water-glycerin mixture has to be matched to the specific model used in the experiment. To this aim the technique suggested by Hopkin et al [5] is used. A mixture slightly richer in glycerin than Geoghegan et al.'s one is prepared, then the model is immersed in the fluid mixture by carefully allowing all of its cavities to be filled by the fluid. A grid of lines is placed behind the model, and while observing the grid distortion water is gradually added to the mixture until the distortion disappears completely. The mixture is thoroughly stirred and pumped through the model each time water is added so that it is homogeneous and homogenously distributed at its inside. Figures 4(a) and 4(b) show the phantom head immersed in a 39% water and 61% glycerin mixture (by volume) and in a 46% water and 54% glycerol mixture (by volume) respectively. The latter is the matching fluid mixture as evidenced by the undistorted rectangular grid visible behind the phantom, figures 4(b). According to equation (2) the matching mixture has n_{mix} =1.407. The mixture density computed from the pure fluids density and the water volume fraction is 1.14 g/cm^3.

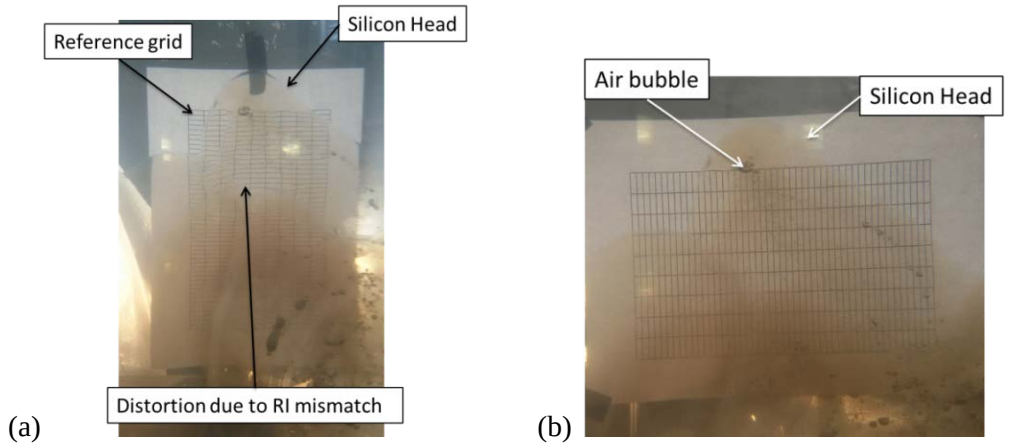

Figure 4. The phantom head immersed in the water/glycerol mixture. (a) Non-matching fluid mixture, (b) matching fluid mixture (46% water and 54% glycerol by volume).

2.3.2. Fluid-dynamic similarity. Being the working fluid not air, there are several differences in the physical parameters between the model and the real phenomenon of human breathing; these differences can be accounted for by obeying dynamical similarity: provided the fluid moves within the model at a suitably scaled velocity, the overall physics is the same and the results can be exactly related to the *in-vivo* values. To this aim the Reynolds number *Re*, equation (3), of the flow phantom is set equal to the real-world flow.

$$Re = \frac{QL}{Av} \tag{3}$$

where Q is the volumetric flow rate, A is the area of a reference section, L is a reference length and v is the kinematic viscosity of the fluid. Considering equation (3) and a geometrical scale factor $M = L_{in-vitro}/L_{in-vivo} = \sqrt{A_{in-vitro}/A_{in-vivo}}$ between the model (*in-vitro*) and the real-world (*in-vivo*) anantomy, the dynamic similarity requires:

$$Q_{in-vitro} = Q_{in-vivo} M \frac{\nu_{in-vitro}}{\nu_{in-vivo}} \tag{4}$$

The dynamic similarity for the oscillatory respiration flow requires the Womersley number α to be taken into account [11]:

$$\alpha = L\sqrt{\frac{\omega}{\nu}} \tag{5}$$

where ω is the angular frequency. To achieve the same Womersley number for the *in-vivo* and the *in-vitro* oscillatory flow conditions, the corresponding time periods $T_{in-vivo}$ and $T_{in-vitro}$ should scale as per Equation (6) [3].

$$= M^2 \frac{\nu_{in-vivo}}{\nu_{in-vitro}} \tag{6}$$

. However in this preliminary work only steady flow conditions are analyzed, thus the Womersley number needs not to be taken into account. The geometrical scale factor of our model is $M=2$. The kinematic viscosity of the matching fluid (46% water and 54% glycerol) at 25 °C is $\nu_{in-vitro}$=5.51×10^{-6} m^2/s, as computed by interpolating the experimental data of Shankar and Kumar [13], while the kinematic viscosity of air at 25 °C and 1 bar is $\nu_{in-vivo}$= 15.58×10^{-6} m^2/s [14]. By substituting those values in equation (4) we get $Q_{in-vitro} = 0.7\ Q_{in-vivo}$.

2.4. *Aquarium and flow system.*
The silicone model is placed in a large container, called the aquarium, having a volume of about 0.33 m^3. Walls providing optical access for the SPIV cameras and the laser sheet are made of optical-grade glass, while the others are made of plexiglass. The glass is used because it has better optical quality and resistance to scratch than plexiglass. The shape of the aquarium is carefully designed to have the viewing angle between the two SPIV camera to form an angle of 90° and the optical axis of each camera to be perpendicular to the glass wall. These angles allow an optimal balance between in-plane and out-of-plane errors in the reconstructed velocity vectors while minimizing the optical distortion [15]. A sketch of the aquarium with the two SPIV cameras is shown in figure 5.

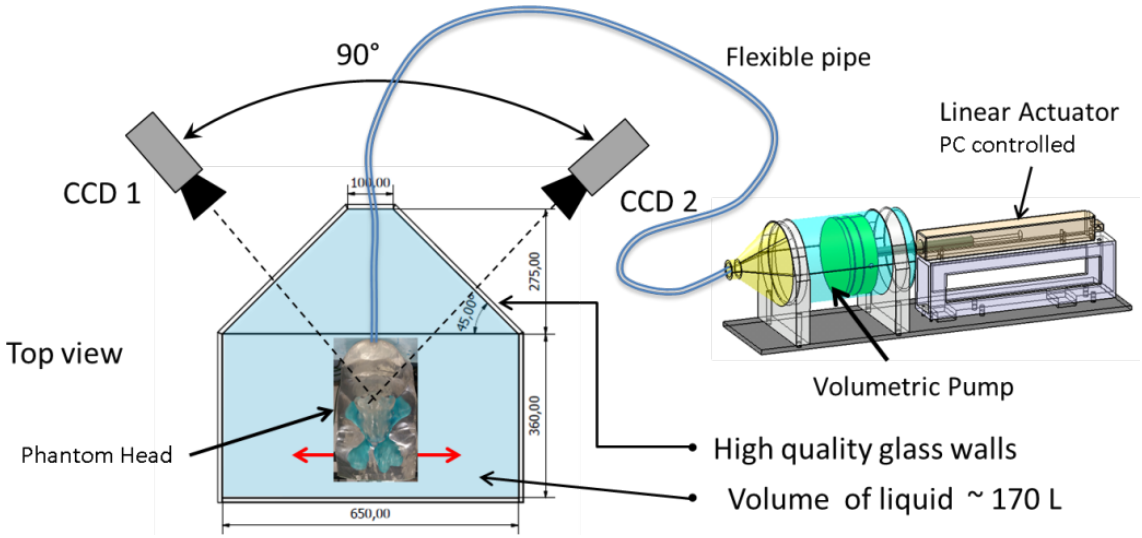

Figure 5. Sketch of the experimental set-up (top view of the aquarium and SPIV camera).

The aquarium is filled with about 170 liters of the matching water/glycerin mixture (46% water and 54% glycerol). The phantom is screwed to an aluminum plate which is placed on a rail system and connected to a linear actuator. This arrangement allows to displace the phantom head respect to the laser sheet and to perform SPIV measurement at different and parallel sagittal planes, figure 6 and figure 7.

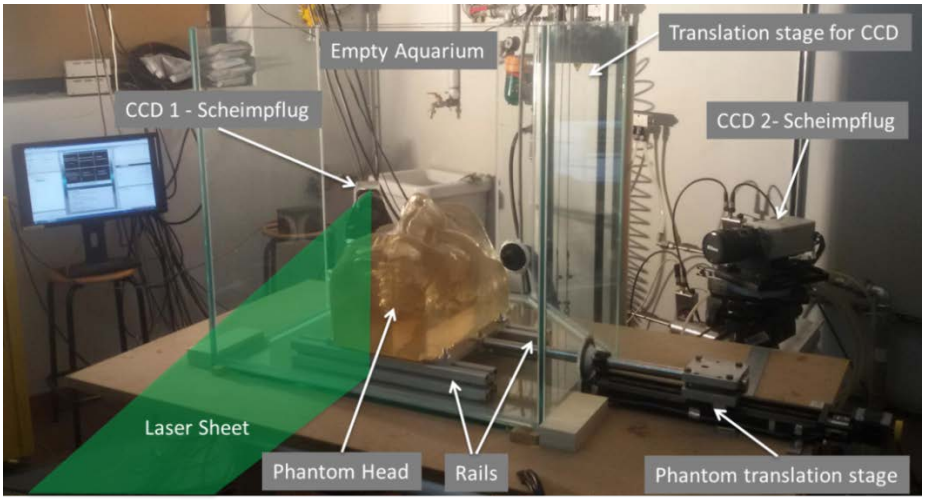

Figure 6. Photograph of the experimental set-up showing the phantom head in the empty aquarium.

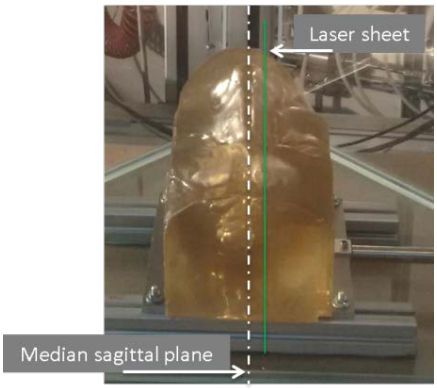

Figure 7. Photograph of the phantom head in the empty aquarium showing the location of the laser sheet during Stereo-PIV measurements.

To implement the scaled version of the human breathing cycle, a pumping system is designed and built on-purpose and connected to the model through a flexible hose. The pump is of syringe type, the piston has a diameter of about 210 mm and a stroke of 100 mm. A linear actuator is connected to the piston and controlled through a PC by using a Labview program. The voltage signal generated by the PC controls speed and acceleration of the piston, thus allowing the scaled periodic breathing cycle of a human being to be accurately reproduced. The pump is connected to the model through a flexible pipe, during the expiratory phase the fluid from the pump is injected through the model and it exhausts in the aquarium through the nose, while the reverse path occurs during the inspiratory phase.

2.5. *Stereo PIV system and measurements.*

A Stereo-PIV system is employed in order to measure the spatial distribution of the three velocity components inside the model. The Stereo-PIV system consisted of a double-pulsed Nd:YAG laser operating at λ = 532 nm with a maximum pulse energy of 200 mJ/pulse and a pair of CCD cameras with a resolution of 1344 * 1024 pixels each, equipped with Nikon lenses of 60 mm focal length, lens aperture was set to F#=8 on both cameras. The cameras were mounted on a traversing system in a Scheimpflug configuration, at opposite sides of the laser sheet. They were oriented with an angle of 45° to the forward scattering direction. The traversing system allowed to move the camera with a resolution of 0.1 mm. The laser sheet was about 1 mm thick and aligned with the sagittal plane of the phantom model. During this preliminary tests, measurements were carried out only in the sagittal plane located about 18 mm away from the median one, see figure 7. Three different fields of view were considered, they were of the same size but displaced each other of 50 mm in the vertical

direction, see figure 8. In the object space each field of view has a size of about 96x54 mm^2 (horizontal x vertical). The velocity maps from those three regions were then recombined together to get the final velocity map.

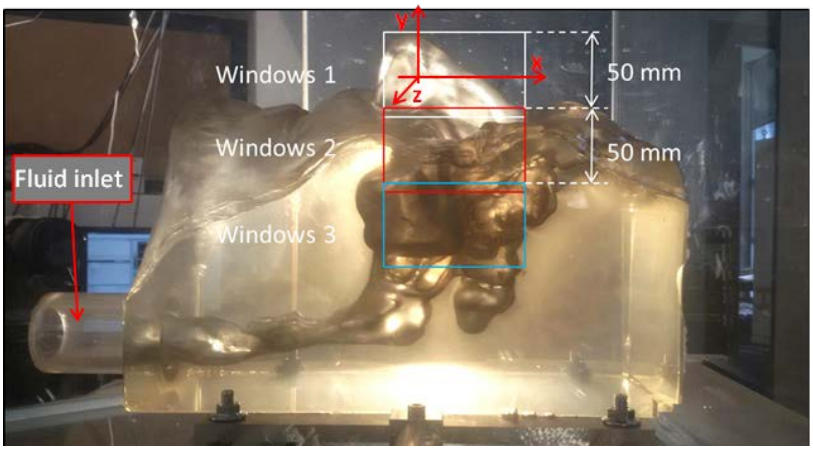

Figure 8. Photo of the phantom model in the empty aquarium showing the reference system and the regions where SPIV measurements have been carried out (the 3 rectangles).

Double images with an inter frame time of 500 μs are acquired at a rate of 5 Hz. Dantec's Dynamic Studio software is used to acquire and to process the images. Before the cross-correlation analysis PIV images are pre-processed. An image balancing filter with a smooth cell size of 5 x 5 is applied to correct the non-uniformities of laser light sheet, then the mean image is computed and subtracted from the instantaneous ones to remove background lighting and reflections.

The seeding particles are polyamide spheres, about 20 μm in diameter, thoroughly dispersed in the liquid mixture. The particle density is about ρ_p= 1.03 g/cm^3 thus slightly buoyant in the fluid mixture (ρ_{mix} = 1.14 g/cm^3). The refractive index of particles is $n_p = 1.5$, not so far from the computed refractive index of the mixture n_{mix} =1.407. The scattered light intensity decreases as the ratio between the refractive index of particles and that of the fluid come close to one, in our case particles were scarcely visible in the SPIV images, this resulted in a quite low image particle density. By increasing the seeding particles dispersed in the fluid the diffused laser light and the liquid turbidity increased deteriorating the SPIV images. Other seeding materials that could improve image quality will be tested in a future work (i.e. metallic coated hollow-glass spheres or fluorescent particles).

During this preliminary tests only a steady flow rate was considered and SPIV images were acquired only during the suction phase of the pump. During such phase the piston moved at a constant velocity of 9 mm/s, the corresponding flow rate of the fluid mixture was about 0.32 l/s. According to equation (4) the latter was dynamically similar to an *in-vivo* air flow rate of about 0.45 l/s. This type of test was planned to verify proper operation of the experimental set-up, it was not intended to simulate an actual breathing cycle which is periodical and composed of inhalation and exhalation phases. The acquisition of PIV images were synchronized with the suction phase of the pump in such a way that measurements were taken only 1.5 seconds after the piston starting and ended about 1.5 seconds before the piston stops. Only about 24 couples of images can be acquired during a single suction phase, thus at each camera position a total of 600 images were collected by replicating the run 25 times.

The standard cross correlation algorithm performed poorly on such images because of the low particle image density and the low brightness of the particle images. Being the flow steady the correlation averaging method [16] implemented in the Dantec's software have been applied to each data set composed by the 600 images. The correlation averaging method is mainly used in micro PIV and it works by averaging the cross-correlation planes of corresponding interrogation areas from different image couples. By this way the uncorrelated noise is rejected while the displacement-

correlation peak is strengthened making the latter visible over the cross-correlation noise floor. The size of the interrogation area (IA) was 32x32 pixels, with an overlap of 75%. The resulting vector spacing was about 0.7 × 0.5 mm^2 ($\Delta x * \Delta y$). The target used for the stereo calibration was an array of dots printed on paper and sandwiched between two thin plexiglass plates. The calibration was performed submerging the target in the aquarium and taking its picture at nine equally spaced positions along the out of plane direction, z ($-2\ mm \leq z \leq 2\ mm$). The implemented camera model was a third order polynomial. The third velocity component was reconstructed from the two 2D vectors fields by using the method proposed by Soloff et al. [17] and implemented in the software.

3. Experimental results

A de-warped mean PIV image corresponding to the field of view indicated as Window 2 in figure 8 is shown in figure 9. The image brightness has been adjusted to enhance the visibility of details. Bright lines in figure 9 correspond to the solid-fluid interface at the laser sheet plane. Such interface is visible due to: a) light scattered by particles attached to the walls, b) a non-perfect index matching between the fluid and the model. The bright silhouette appearing in the mean image was used as a reference to manually draw a mask. The latter was subsequently applied to the velocity maps to highlight the non-fluid region. Laser light sheet non-uniformity (shown as black stripes) and light diffused by model defects or damages are also visible in figure 9. The image balancing and background removal procedures describe in section 2.5 allowed to partially compensate for such image defects.

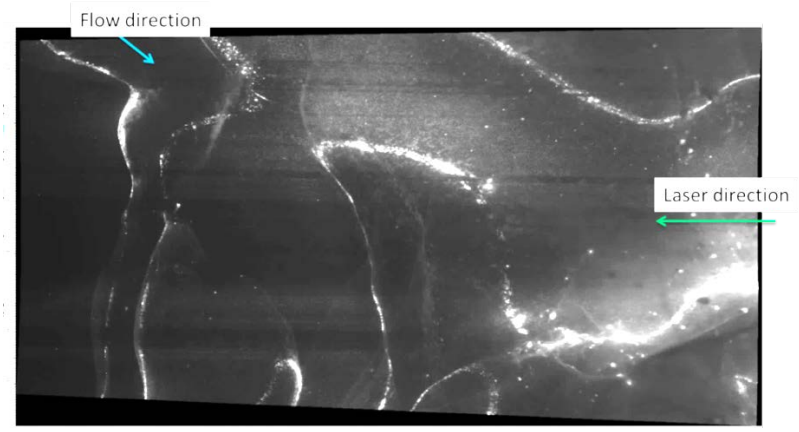

Figure 9. De-warped mean PIV image, the field of view corresponds to windows 2 in figure 8.

The velocity map (modulus of the velocity vector) obtained from the Stereo-PIV measurements is shown in figure 10(a), and compared to numerical results shown in figure 10(b).

The numerical data have been obtained via a computational procedure developed during the last few years at Politecnico di Milano, which is entirely based on open-source software. The data are taken from one case among the several considered in previous work (more details can be found in [18] and [19]), is based on the same anatomy, and portraits the same mean velocity field as computed from a Large-Eddy Simulation. The simulation has been carried out on the real model (i.e. 1:1 scale, working fluid is air), and a correction factor has been subsequently applied to the velocity and length scales in order to produce figure 10, accounting for the dynamical similarity between the two flows. The data presented correspond to a mean flow field computed via time-averaging of the unsteady and 3-dimensional LES results, for a steady inspiration, hence directly comparable to the experiment. The numerical calculations covered 0.2 seconds of physical time, and the computing time required for such a case was of approximately 100 hours by using 16 computing cores. The mesh size, of more than 5M elements, makes this LES a very well resolved one, so that the contribution from the turbulence model (the classical, non-dynamic Smagorinsky model) is almost negligible everywhere. All the terms of the incompressible Navier-Stokes equations have been discretized via second-order-accurate operators.

The mean flow field plotted in figure 10(b) is the time-average of the time-varying LES solution over the entire simulation time. The experimental velocity maps from the three fields of view of figure 8 are plotted in figure 10(a) as a single map by taking into account the vertical displacement of 50 mm existing between each of them; on the same figure, the dashed area highlight the non-fluid region. Despite the use of the correlation averaging method, regions exist where clearly the fluid velocity cannot be recovered. These regions appear as stripes in the velocity maps, and they seem to overlap with the black stripes observed in the laser sheet, see figure 9. The latter indicate regions less lighted by the laser sheet, where particles images are more faint, thus exacerbating the issue related to the low image particle density and decreasing the number of validated velocity vectors. From the figure, one can easily appreciate the complexity of the flow patterns that develop in such small-scale domain. In figure 10(b), the same plot as derived from CFD shows a similar picture, at least at a qualitative level. Local velocity maxima in correspondence of the 3 meata, where the cross-section of the nasal airways shrinks owing to the protrusion of the turbinates, can be clearly observed.

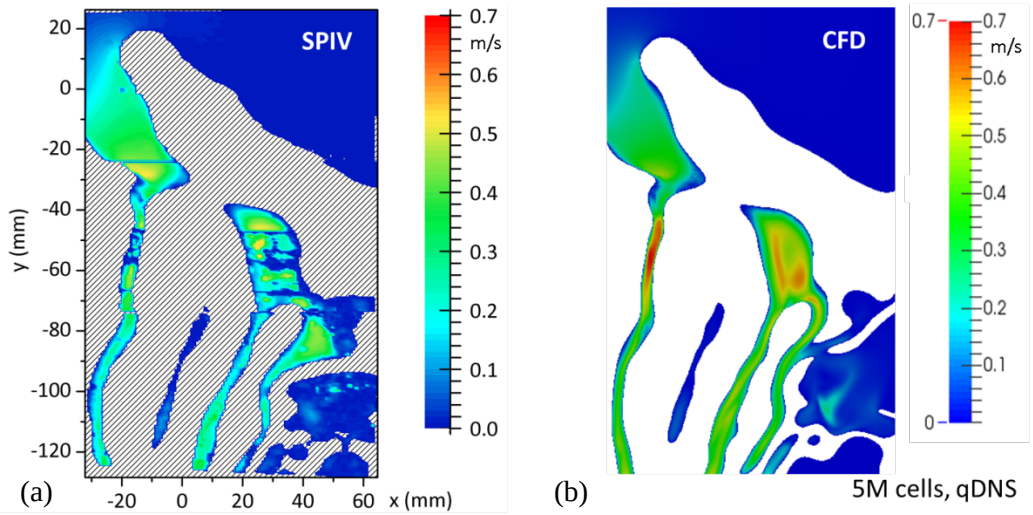

Figure 10. Modulus of the velocity vector in the sagittal plane z=18 mm. (a) SPIV measurements, (b) LES numerical simulation (mean flow).

4. Conclusion

This paper describes an experimental set-up based on Stereo-PIV and refractive index matching techniques used to analyze the flow inside a complete patient-specific silicon model of the human nose. The geometry of the model reproduces that obtained through a CT scan and then used in the numerical simulations. The model has been built in a 2:1 scale and using 3D printing technology. To the authors' knowledge, this is the first attempt to experimentally investigate the flow inside a complete human nose including all the paranasal sinuses. The making of the phantom model and the choice and tuning of the matching fluid mixture are thoroughly described in the paper. The fluid dynamic similitude is also briefly presented and discussed. An aquarium of about 0.33 m^3 having suitable optical accesses for laser and camera has been built and filled with about 170 liters of matching fluid mixture. The phantom model is submerged in the aquarium and it is connected to a piston pump through a flexible pipe that enters in the model upstream of the laryngopharynx: this allows the fluid mixture to be inhaled/exhaled through the nose to simulate the breathing cycle. Few preliminary test were performed using a constant flow rate to verify proper operation of the experimental set-up. Those tests were not intended to simulate an actual breathing cycle which is periodical and composed of inhalation and exhalation phases. A stereo-PIV system allowed to measure the three velocity components at three different location in a sagittal plane of the phantom model. Experimental results evidenced that for this quite large model the refractive index matching worked properly and that the set-up was suitable for the intended purposes. They also evidenced that seeding

particles having higher light scattering capability should be sought, alternatively fluorescent seeding could also be used. Finally, despite the preliminary stage of the research, the measured flow field resulted in fair agreement with that obtained by a LES simulation on the same anatomy.

Acknowledgments
The authors wish to thank the collaborators who contributed to the present work, namely MD Carlotta Pipolo and Alberto Saibene, and Mr. Simone Raina and Mr. Martino Ermacora.
Financial support from Regione Lombardia and Italian Ministry of Health through the project CAPNAF-FD is gratefully acknowledged.

References

[1] Stewart M, Ferguson B J and Fromer L 2010 Epidemiology and burden of nasal congestion Int. J. Gen. Med. 3 37–45
[2] Smith K A, Orlandi R R and Rudmik L 2015 Cost of adult chronic rhinosinusitis: A systematic review Laryngoscope 125 1547–56
[3] Spence C J T, Buchmann N A, Jermy M C and Moore S M 2011 Stereoscopic PIV measurements of flow in the nasal cavity with high flow therapy Exp. Fluids 50 1005–17
[4] Im S, Heo G E, Jeon Y J, Sung H J and Kim S K 2014 Tomographic PIV measurements of flow patterns in a nasal cavity with geometry acquisition Exp. Fluids 55
[5] Hopkins L M, Kelly J T, Wexler a. S and Prasad a. K 2000 Particle image velocimetry measurements in complex geometries Exp. Fluids 29 91–5
[6] Budwig R 1994 Refractive index matching methods for liquid flow investigations Exp. Fluids 17 350–5
[7] Wiederseiner S, Andreini N, Epely-Chauvin G and Ancey C 2011 Refractive-index and density matching in concentrated particle suspensions: a review Exp. Fluids 50 1183–206
[8] Amini N and Hassan Y A 2012 An investigation of matched index of refraction technique and its application in optical measurements of fluid flow Exp. Fluids 53 2011–20
[9] Pieper S, Halle M and Kikinis R 2004 3D Slicer 2004 2nd IEEE Int. Symp. Biomed. Imaging Nano to Macro (IEEE Cat No. 04EX821) 2 632–5
[10] Dow Corning 2014 Product Information of Sylgard® 184 Silicone Elastomer 4
[11] Geoghegan P H, Buchmann N A, Spence C J T, Moore S and Jermy M 2012 Fabrication of rigid and flexible refractive-index-matched flow phantoms for flow visualisation and optical flow measurements Exp. Fluids 52 1331–47
[12] Vural U S, Muradoglu V and Vural S 2011 Excess molar volumes, and refractive index of binary mixtures of glycerol + methanol and glycerol + water at 298.15 k and 303.15 K Bull. Chem. Soc. Ethiop. 25 111–8
[13] Shankar P N and Kumar M 1994 Experimental Determination of the Kinematic Viscosity of Glycerol-Water Mixtures Proc. R. Soc. London A Math. Phys. Eng. Sci. 444
[14] Spurk J H and Aksel N 2012 Fluid mechanics
[15] Prasad a. K 2000 Stereoscopic particle image velocimetry Exp. Fluids 29 103–16
[16] Westerweel J, Elsinga G E and Adrian R J 2013 Particle Image Velocimetry for Complex and Turbulent Flows Annu. Rev. Fluid Mech. 45 409–36
[17] Soloff S M, Adrian R J and Liu Z-C 1997 Distortion compensation for generalized stereoscopic particle image velocimetry Meas. Sci. Technol. 8 1441–54
[18] Manara F and Lamberti G 2015 Simulazioni RANS and LES delle cavità nasali Master's Thesis in Aeronautical Engineering (Politecnico di Milano)
[19] Lamberti G, Manara F and Quadrio M 2015 RANS/LES/DNS simulations of the airflow in nasal cavities APS Division of Fluid Dynamics (Fall) 2015